



1

2

3 **Comparison of Optimal Estimation HDO/H<sub>2</sub>O Retrievals**

4 **from AIRS with ORACLES measurements**

5 **Robert L. Herman<sup>1</sup>, John Worden<sup>1</sup>, David Noone<sup>2</sup>, Dean Henze<sup>2</sup>, Kevin  
6 Bowman<sup>1</sup>, Karen Cady-Pereira<sup>3</sup>, Vivienne H. Payne<sup>1</sup>, Susan S. Kulawik<sup>4</sup>, and  
7 Dejian Fu<sup>1</sup>**

8 [1] Jet Propulsion Laboratory, California Institute of Technology, Pasadena, California,  
9 USA.

10 [2] College of Earth, Ocean, and Atmospheric Sciences, Oregon State University,  
11 Corvallis, Oregon, USA.

12 [3] Atmospheric and Environmental Research, Inc. (AER), Lexington, Massachusetts,  
13 USA.

14 [4] Bay Area Environmental Research Institute, Petaluma, California, USA.

15 Correspondence to: R. L. Herman ([Robert.L.Herman@jpl.nasa.gov](mailto:Robert.L.Herman@jpl.nasa.gov))

16



17    **Abstract**

18    In this paper we evaluate new retrievals of the deuterium content of water vapor from the  
19    Aqua Atmospheric InfraRed Sounder (AIRS) with aircraft measurements of HDO and  
20    H<sub>2</sub>O from the ObseRvations of Aerosols above Clouds and their intEractionS  
21    (ORACLES) field mission. Single footprint AIRS radiances are processed with an  
22    optimal estimation algorithm that provides a vertical profile of the HDO/H<sub>2</sub>O ratio,  
23    characterized uncertainties, and instrument operators (or averaging kernel matrix). These  
24    retrievals are compared to vertical profiles of the HDO/H<sub>2</sub>O from the Oregon State  
25    University Water Isotope Spectrometer for Precipitation and Entrainment Research  
26    (WISPER) on the ORACLES NASA P-3B Orion aircraft. Measurements were taken over  
27    the Southeast Atlantic Ocean from 31 August to 25 September 2016. HDO/H<sub>2</sub>O is  
28    commonly reported in  $\delta D$  notation, which is the fractional deviation of the HDO/H<sub>2</sub>O  
29    ratio from the standard reference ratio. For collocated measurements, the satellite  
30    instrument operator (averaging kernels and a priori constraint) is applied to the aircraft  
31    profile measurements. We find that AIRS  $\delta D$  bias relative to the aircraft is well within  
32    the estimated measurement uncertainty. In the lower troposphere, 1000 to 800 hPa, AIRS  
33     $\delta D$  bias is -6.6‰ and the Root Mean Square (RMS) deviation is 20.9‰, consistent with  
34    the calculated uncertainty of 19.1‰. In the mid-troposphere, 800 to 500 hPa, AIRS  $\delta D$   
35    bias is -6.8‰ and RMS 44.9‰, comparable to the calculated uncertainty of 25.8‰.



36    **1. Introduction**

37    The deuterium content of tropospheric water vapor is sensitive to the different types of  
38    atmospheric moisture sources such as evaporation from the ocean or land and the  
39    processing that occurs during transport such as mixing or condensation (e.g., Craig, 1961;  
40    Dansgaard, 1964; Galewsky et al., 2016). Condensation and precipitation preferentially  
41    remove the heavier HDO isotopologue from the gas phase relative to the parent  
42    isotopologue H<sub>2</sub>O, whereas evaporation of precipitation at lower altitudes in the  
43    atmosphere can enrich HDO relative to H<sub>2</sub>O vapor. These unique, isotopic properties  
44    allow HDO/H<sub>2</sub>O to be a tracer for the origin, condensation and evaporation history of an  
45    air parcel, thus useful for evaluating changes to the water cycle (e.g., Worden et al., 2007;  
46    Noone, 2012; Galewsky et al., 2016).

47

48    In the last decade, satellite retrievals of the isotopic composition of tropospheric water  
49    vapor (HDO and H<sub>2</sub>O) have been developed, including Envisat/SCIAMACHY (Scanning  
50    Imaging Absorption Spectrometer for Atmospheric Chartography) (Frankenberg et al.,  
51    2009), IASI (Infrared Atmospheric Sounding Interferometer) aboard the MetOp satellites  
52    (Herbin et al., 2009; Schneider and Hase, 2011; Lacour et al., 2012), and TES (the  
53    Tropospheric Emission Spectrometer) on the Aura spacecraft (Worden et al., 2006;  
54    Worden et al., 2007). More recently, Worden et al. have developed HDO retrievals from  
55    the Aqua Atmospheric InfraRed Sounder (AIRS) single footprint Level 1b radiance data  
56    (Worden et al., 2019). These AIRS retrievals are the subject of the present comparison  
57    with aircraft data.

58



59 Satellite HDO measurements have been utilized to study tropical carbon/water feedbacks  
60 (Wright et al., 2017), moist processes in deep convection (e.g. Worden et al., 2007), and  
61 the global partitioning of transpiration to evapotranspiration (Good et al., 2015). A  
62 decadal record of HDO has promise in characterizing global shifts in moisture sources  
63 and atmospheric water balance in response to warming, climactic variability, and land-  
64 use. For example, Bailey et al. (2017) shows that a record of free-tropospheric HDO/H<sub>2</sub>O  
65 would provide an observational constraint on changes in the tropical water balance  
66 (evaporation minus precipitation) in response to shifts in ocean temperature. Wright et al.  
67 (2017) also shows that free-tropospheric deuterium measurements provide a fundamental  
68 new constraint in carbon / water dynamics in the Amazon. They use the TES isotope  
69 measurements to show that dry-season evapotranspiration is critical towards initiating the  
70 southern Amazon rainfall, which in turn is critical towards sustaining the Amazon  
71 rainforest (Fu et al., 2013). For these reasons a record of the deuterium content of water  
72 vapor from the long (17 years and continuing) record from AIRS holds significant  
73 potential to evaluate changes in the global water cycle.

74

75 This paper presents detailed comparisons between new AIRS measurements of the  
76 deuterium content of water vapor (or HDO/H<sub>2</sub>O ratio) and accurate *in situ* HDO/H<sub>2</sub>O  
77 measurements from an aircraft sensor during the NASA ObseRvations of Aerosols above  
78 Clouds and their intEractiOnS (ORACLES) field mission. In this paper, we denote the  
79 volume mixing ratios  $q_D$  for HDO, and  $q_H$  for H<sub>2</sub>O. By standard convention, we report  
80 the isotopic abundance as  $\delta D$  (per mil or ‰) =  $[(q_D/q_H)_{obs}/(q_D/q_H)_{std} - 1] * 1000$ ,



81 where  $(q_D/q_H)_{std} = 3.11 \times 10^{-4}$  based on the D/H standard ratio for Vienna Standard Mean  
82 Ocean Water (SMOW).

83

84 **2. Instrumentation**

85 **2.1 AIRS Instrument Description**

86 The Atmospheric InfraRed Sounder (AIRS) on the NASA Aqua satellite is a nadir-  
87 viewing, scanning thermal infrared grating spectrometer that covers the 3.7 to 15.4  $\mu\text{m}$   
88 spectral range with 2378 spectral channels (Pagano et al., 2003, and Aumann et al.,  
89 2003). Launched on May 4, 2002, Aqua is in a sun-synchronous orbit at 705 km with an  
90 approximately 1:30 pm equator crossing-time as part of the A-Train satellite  
91 constellation. AIRS continues to make daily measurements of most of the globe with its  
92 wide cross-scanning swath of coverage. The AIRS instrument makes collocated  
93 measurements with the Advanced Microwave Sounding Unit (AMSU) on the Aqua  
94 satellite. There are nine AIRS single footprint observations (nadir horizontal resolution of  
95  $\sim 13.5$  km) arranged in a 3 by 3 grid within a single AMSU footprint of  $\sim 45$  km (Aumann  
96 et al., 2003). For HDO retrievals, the single footprint AIRS Level 1b (L1b) radiances are  
97 utilized. Absolute radiometric accuracy between 220 K and 320 K at all observation  
98 angles is better than 0.2 K (Pagano et al., 2003, 2008). The algorithm applied to AIRS  
99 radiances to yield HDO is described below in Sect. 3.1.

100

101 **2.2 WISPER system for aircraft measurements**

102 Aircraft measurements were made on the NASA P-3B Orion aircraft during the NASA  
103 ORACLES field mission. ORACLES is a five-year Earth Venture Suborbital (EVS-2)



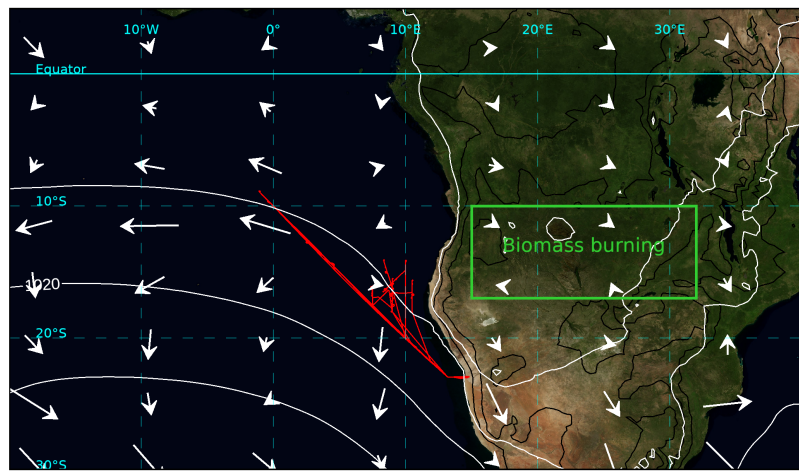
104 investigation with three Intensive Observation Periods (IOP) designed to study key  
105 processes that determine the climate impacts of African biomass burning aerosols in  
106 2016, 2017, and 2018. The ORACLES experiment provided multi-year airborne  
107 observations from the NASA P-3B Orion and ER-2 aircraft over the complete vertical  
108 column of the key parameters that drive aerosol-cloud interactions in the southeast  
109 Atlantic Ocean region. The focus of the ORACLES field measurements was a biomass  
110 burning plume that advected west from the African continent to the lower troposphere (at  
111 2 to 5 km above sea level, ASL) above the Atlantic Ocean. Here we use data from the  
112 ORACLES 2016 IOP (ORACLES Science Team, 2017), and report on aircraft versus  
113 satellite comparisons from eight flights (Fig. 1 and Table 1).

114

115 Water vapor isotopic abundances ( $\text{HDO}/\text{H}_2\text{O}$  and  $\text{H}_2^{18}\text{O}/\text{H}_2^{16}\text{O}$ ) were measured in situ on  
116 the aircraft with the Oregon State Water WISPER system (Water Isotope Spectrometer  
117 for Precipitation and Entrainment Research, Henze et al., in prep.), which uses a modified  
118 commercial Picarro L2120-i  $\delta\text{D}/\delta^{18}\text{O}$  Ultra High-Precision Isotopic Water Analyzer. The  
119 measurement technique is cavity ring-down (CRD) spectroscopy (O'Keefe and Deacon,  
120 1988; Berden et al., 2000; Gupta et al., 2009). The majority of measurements analyzed in  
121 this paper are located within the biomass burning plume, characterized by elevated  $\text{H}_2\text{O}$   
122 (approximately 6000 ppmv) and elevated  $\delta\text{D}$  (-100 to -70‰). At these abundances of  
123  $\text{HDO}/\text{H}_2\text{O}$ , the 1-Hz precision ( $1\sigma$ ) of the measurements of  $\delta\text{D}$  is  $\pm 3\text{\textperthousand}$ , and the accuracy  
124 is  $\pm 6.5\text{\textperthousand}$ .

125

126



127

128 **Figure 1.** Selected flight tracks (red lines) of the NASA P-3B Orion aircraft during the  
129 ORACLES 2016 IOP used in this study, with corresponding flight dates listed in Table 1.  
130 Also shown is the biomass burning region (green rectangle), 700 hPa winds (white  
131 vectors), and surface pressure (white isobars).

132

133 **Table 1.** Summary of matches AIRS and WISPER  $\delta D$  measurements during NASA ORACLES\*.

| Flight Date | Daily Number of<br>Matched Profiles, loose<br>lat/lon constraint. | Daily Number of<br>Matched Profiles, tighter<br>lat/lon constraint. |
|-------------|---|---|
| 31-Aug-2016 | 138   | 26  |
| 2 Sep 2016  | 15  | 15  |



|              |            |            |
|--------------|------------|------------|
| 4 Sep 2016   | 102        | 26         |
| 10 Sep 2016  | 48         | 7          |
| 12 Sep 2016  | 18         | 4          |
| 14 Sep 2016  | 12         | 5          |
| 20 Sep 2016  | 11         | 4          |
| 25 Sep 2016  | 102        | 23         |
| <b>Total</b> | <b>446</b> | <b>110</b> |

134 \*NASA ORACLES is the “ObseRvations of Aerosols above Clouds and their intEractioN” Earth Venture  
135 Suborbital Mission.  
136

### 137 **3 Satellite Retrieval**

#### 138 **3.1 Retrieval Algorithm**

139 The single footprint AIRS HDO profile data used in this work were produced using the  
140 retrieval algorithm, named the Multi-SpEctra, Multi-SpEcies, Multi-Sensors (MUSES)  
141 algorithm (Fu et al., 2013, 2016, 2018; Worden et al., 2019). The MUSES algorithm can  
142 use radiances from multiple instruments including AIRS and other instruments (CrIS,  
143 TES, OMI, OMPS, TROPOMI, and MLS) to quantify geophysical observables that affect  
144 the corresponding radiance. The AIRS single footprint HDO profile retrievals have been  
145 described by Worden et al. (2019), and have heritage from the TES algorithm (Worden et  
146 al., 2004, 2006, 2007, 2011, 2012, 2013; Bowman et al. 2006, 2002). The Optimal  
147 Spectral Sampling (OSS) fast radiative transfer model (Moncet et al., 2008, 2015) for  
148 single footprint AIRS measurements has been integrated into the MUSES algorithm, in  
149 support of the operational data production towards the multi-decadal record of global  
150 HDO profiles. The supplement attached to this paper discusses the sensitivity of the  
151 retrievals to the choice of forward model. The retrieval uses the optimal estimation  
152 method to quantify atmospheric HDO and H<sub>2</sub>O (Worden et al. 2006, 2012, 2019). For



153 both AIRS and TES retrievals, height discrimination of the HDO/H<sub>2</sub>O ratio in the  
154 troposphere is provided by spectral resolution of pressure and temperature broadened  
155 absorption features of their corresponding lines (Beer et al., 2002). The algorithms and  
156 spectral microwindows are described by Worden et al. (2019). Chemical species CH<sub>4</sub>,  
157 CO, HDO, and H<sub>2</sub>O are jointly retrieved along with atmospheric temperature, surface  
158 temperature, land emissivity and clouds (Worden et al. 2012). The retrieval optimizes the  
159 ratio of HDO to H<sub>2</sub>O, as opposed to either HDO or H<sub>2</sub>O alone (Worden et al., 2019,  
160 2012, 2006). AIRS radiances at wavelengths from 8 to 12  $\mu\text{m}$  are used here, excluding  
161 the 9.6  $\mu\text{m}$  ozone band. The parent molecule H<sub>2</sub>O is retrieved at both 8 and 12  $\mu\text{m}$ , but  
162 HDO is retrieved primarily from strong absorption lines in the 8  $\mu\text{m}$  region (particularly  
163 in the wavenumber range 1210 to 1270  $\text{cm}^{-1}$ ). Cloud optical depth and cloud top pressure  
164 are jointly retrieved with the chemical species, using the approach described in Kulawik  
165 et al. (2006). The cloud-clearing approach (Susskind et al., 2003), utilized in AIRS  
166 operational products up to and including AIRS v6, where retrievals are reported on the 45  
167 km AMSU footprint, is not utilized here. As described by Worden et al. (2019), retrievals  
168 are performed on single AIRS 13.5-km footprints in order to preserve the Level 1B  
169 radiance noise characteristics (Irion et al., 2018; DeSouza et al., 2018).

170

171 For H<sub>2</sub>O, the a priori constraint vectors come from NASA's Goddard Earth Observing  
172 System (GEOS) data assimilation system GEOS version 5.12.4 processing stream  
173 (Rienecker et al., 2008). These are produced by the Global Modeling and Assimilation  
174 Office (GMAO) at the NASA Goddard Space Flight Center (GSFC). The GMAO GEOS-  
175 5.12.4 water mixing ratios are linearly interpolated to the latitudes, longitudes, and



176 log(pressure) levels of satellite retrievals to generate the a priori profiles.  
177  
178 For all HDO retrievals, the initial profile of the HDO/H<sub>2</sub>O<sup>16</sup>O isotopic ratio is set equal to a  
179 simulated tropical profile (Worden et al., 2006). In the AIRS HDO product files, a priori  
180 HDO is defined as the product of the local a priori H<sub>2</sub>O profile (GMAO GEOS-5.12.4)  
181 and one tropical a priori profile of the HDO/H<sub>2</sub>O isotopic ratio (Worden et al., 2006). The  
182 initial guess profiles for H<sub>2</sub>O are set equal to the a priori.

183

184 **3.2 Method of comparison**

185 The AIRS HDO/H<sub>2</sub>O retrievals are matched up in space and time with the aircraft in situ  
186 HDO/H<sub>2</sub>O measurements. A critical aspect of validating satellite retrievals is obtaining  
187 data that span the altitudes where the satellite has sensitivity to HDO/H<sub>2</sub>O. AIRS data are  
188 sensitive to the HDO/H<sub>2</sub>O ratio in the atmosphere from the surface up to approximately  
189 10,000 m altitude. The aircraft samples HDO and H<sub>2</sub>O from the surface up to 6000 m  
190 altitude, spanning most of the altitudes where the AIRS data are sensitive and therefore  
191 allowing us to validate AIRS HDO/H<sub>2</sub>O with in situ measurements.

192

193 For direct comparison of AIRS HDO/H<sub>2</sub>O with in situ HDO/H<sub>2</sub>O, the AIRS instrument  
194 operator (averaging kernel and *a priori* constraint) is applied to the in situ data (see Eq. 1  
195 below), as described by Rodgers (2000). This has the effect of smoothing the in situ data  
196 to the same resolution as the satellite retrievals. The averaging kernel matrix  $A$  is the  
197 sensitivity of the AIRS estimate to the true concentration in the atmosphere (Rodgers,  
198 2000). The in situ profile with applied averaging kernel  $x_{insituw/AK}$  is calculated jointly for



199 HDO and H<sub>2</sub>O using the AIRS operator:

200  $x_{insituw/AK} = x_a + A_{xx}(x - x_a)$  (1)

201

202 Joint HDO/H<sub>2</sub>O retrievals are performed on the logarithm of the volume mixing ratios,  $x_D$   
203 = ln( $q_D$ ) and  $x_H$  = ln( $q_H$ ) (Worden et al., 2012, 2006). The data structure for AIRS HDO  
204 files is similar to TES HDO, with details provided by Herman et al. (2014).

205

206 For comparison with AIRS, the in situ HDO and H<sub>2</sub>O profiles are extended to cover the  
207 full range of AIRS levels. In the boundary layer, from the surface up to the lowest  
208 altitude aircraft data, we assume constant values of HDO and H<sub>2</sub>O set equal to the first  
209 aircraft measurement. In the range of aircraft data (up to 6000-m flight ceiling), the  
210 aircraft in situ HDO and H<sub>2</sub>O data are interpolated to the levels of the AIRS forward  
211 model, smoothing fine scale features. In the layers above the aircraft maximum altitude,  
212 the profile is extrapolated using a scaled a priori profile. In this paper, all comparisons  
213 have been completed applying Eq. 1.

214

#### 215 **4 Validation**

216 Validating the accuracy of AIRS HDO and H<sub>2</sub>O retrievals is important for studies of the  
217 hydrologic cycle, exchange processes in the troposphere, and climate change.  
218 Comparisons of AIRS and TES over five years (2006-2010) indicate that the retrieval  
219 characteristics of the AIRS HDO/H<sub>2</sub>O measurements have similar vertical resolution and  
220 uncertainty in the middle troposphere but with slightly less sensitivity in the lower  
221 troposphere (Worden et al., 2019). Worden et al. (2019) reported that the calculated



222 uncertainty of AIRS HDO/H<sub>2</sub>O is ~30 per mil for a tropospheric average between 750  
223 and 350 hPa, with mean bias between TES and AIRS (TES-AIRS) for the HDO/H<sub>2</sub>O  
224 ratio of ~-2.6 per mil and a latitudinal variation of ~7.6 per mil.

225

226 **4.1 Comparison of AIRS with Aircraft Measurements**

227 **ORACLES 8/31 to 9/25/2016 data comparison.**

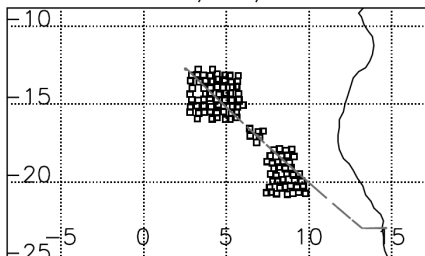
228 In this section, we describe comparisons between AIRS and ORACLES aircraft HDO  
229 measurements. First, time segments of each aircraft flight are identified where the aircraft  
230 profiled from the boundary layer up to approximately 6000 m altitude. To minimize the  
231 impact of atmospheric spatial and temporal variability, same-day AIRS measurements are  
232 selected for the same latitude/longitude rectangle as each aircraft profile (Fig. 2). These  
233 matched pairs are compared by the method described in Sect. 3.2. Within each flight are  
234 several profiles each spanning 1 to 3 degrees (or ~ 100 to 300 km), so measurement pairs  
235 are typically within 3 degrees (Fig. 2). The standard data retrieval quality flags for the  
236 retrieval are used in this analysis, which are based on the Aura TES data retrieval quality  
237 flags (Herman and Kulawik, 2018). For closer spatial coincidence, we also selected  
238 AIRS-aircraft measurement pairs within 0.3 degrees (Fig. 3). Following Worden et al.  
239 (2007) and Brown et al. (2008), we filter data for a reasonable threshold of DOFS (DOFS  
240 > 1.1), but include all cloud optical depths. Fig. 4(a) shows a representative 31 Aug 2016  
241 comparison between aircraft water vapor δD from WISPER and the coincident AIRS  
242 retrieval. Fig. 4(b) shows the corresponding averaging kernels.

243

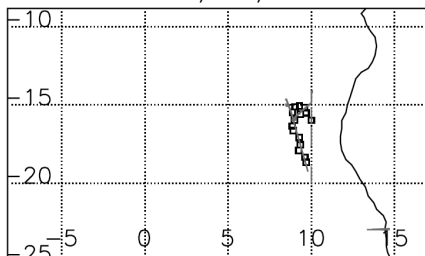


244

2016/08/31

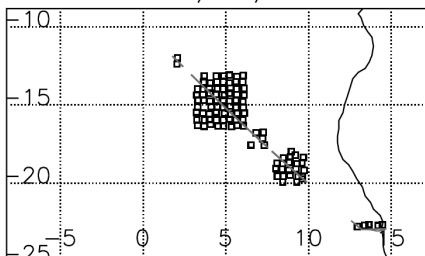


2016/09/02

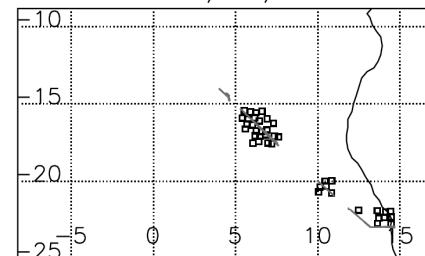


245

2016/09/04

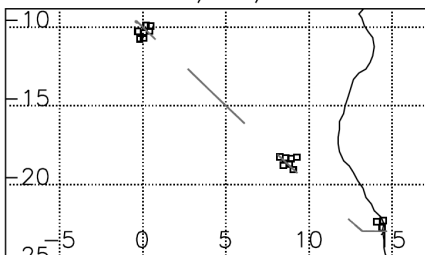


2016/09/10

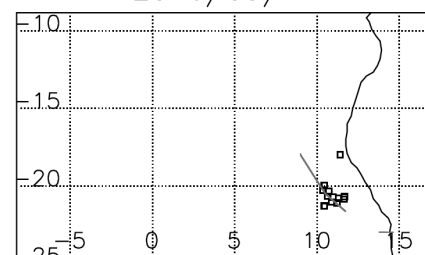


246

2016/09/12



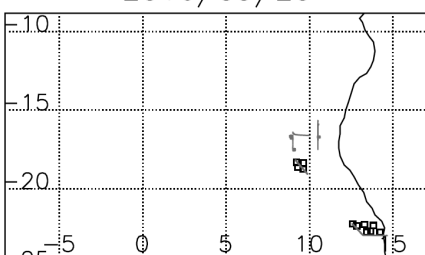
2016/09/14



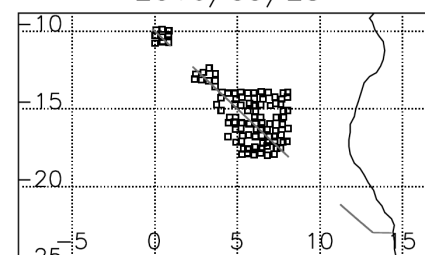
247

248

2016/09/20



2016/09/25



249

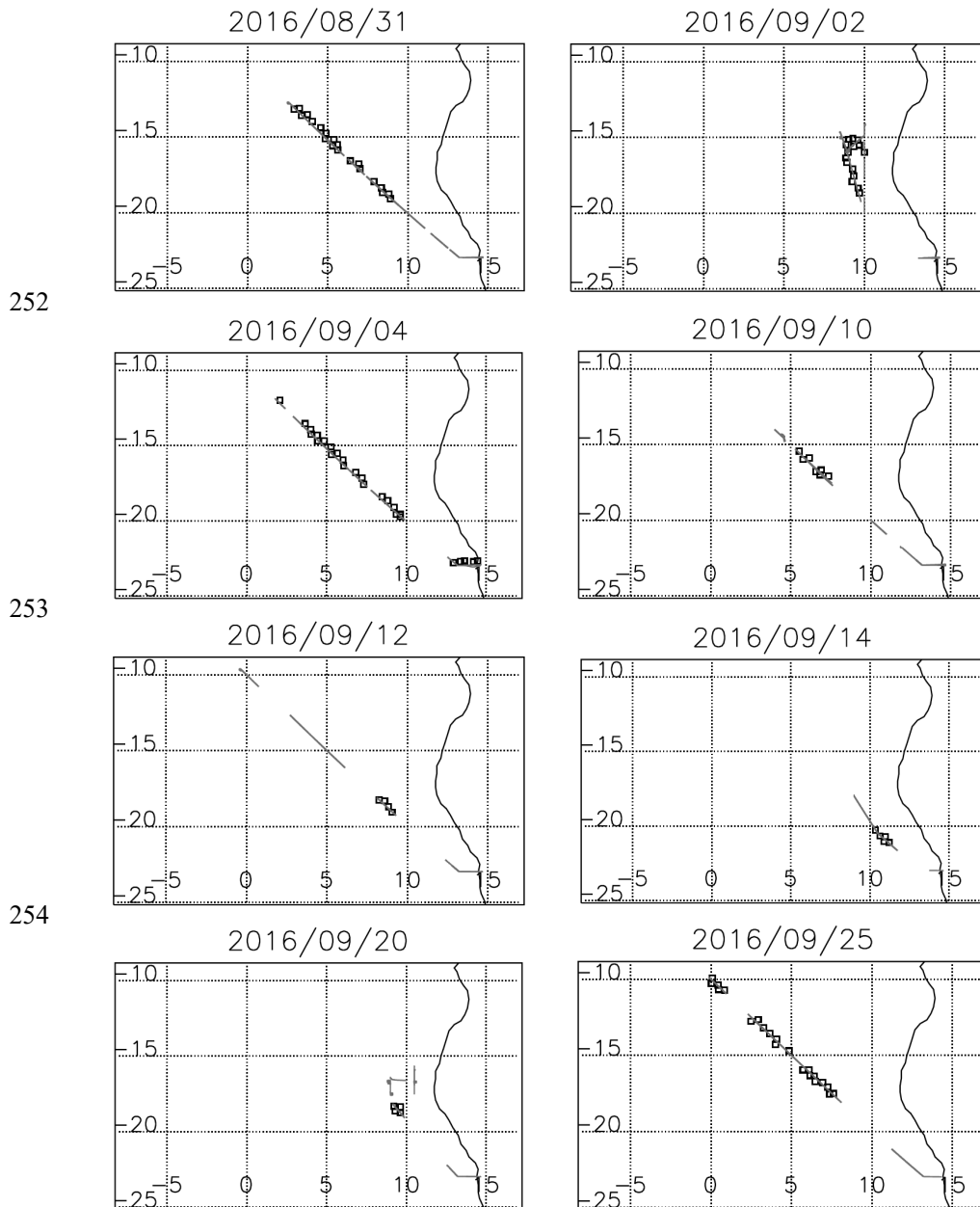
**Figure 2.** ORACLES aircraft profiles (thin grey line segments) over the southeast

250

Atlantic Ocean to the west of Africa are matched to AIRS fields of view (FOVs) (square symbols) within the same latitude/longitude rectangle as the aircraft profiles for eight



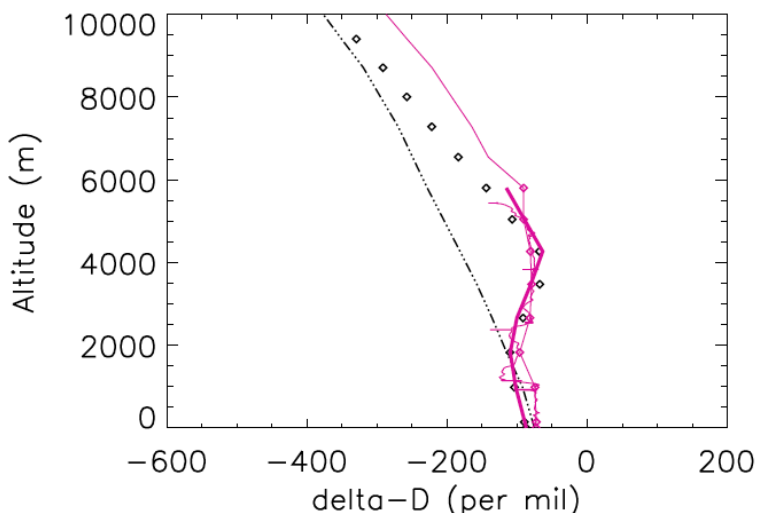
251 flights in 2016.



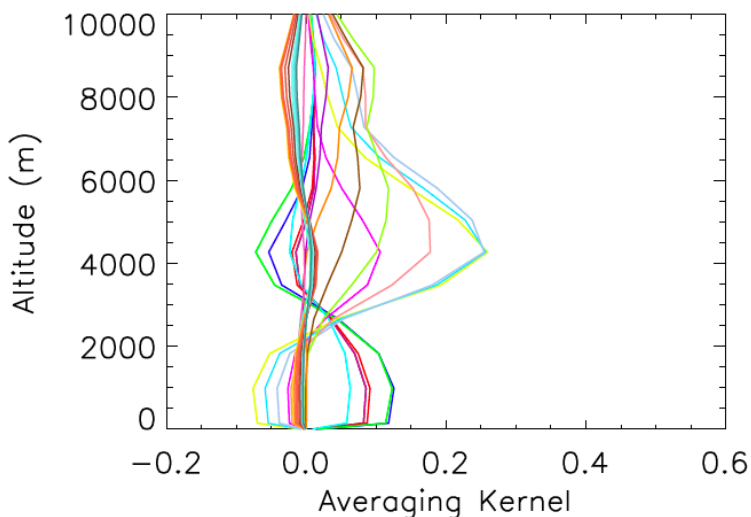
256 **Figure 3.** In close spatial coincidence, ORACLES aircraft profiles (thin grey line  
257 segments) are matched within 0.3 degrees to AIRS FOVs (square symbols).



258



259



260

261 **Figure 4. (a)** Sample comparison of the  $\delta D$  profiles by aircraft and satellite over the  
262 southeast Atlantic Ocean during ORACLES on 31 August 2016: shown are AIRS  $\delta D$   
263 (black diamond symbols), the prior  $\delta D$  (black dash-dot-dot line), nearest WISPER  $\delta D$   
264 (thin red line), WISPER  $\delta D$  interpolated to satellite levels (red diamonds), and the  
265 WISPER  $\delta D$  with the AIRS averaging kernel applied (thick red line).



266   **(b)** Averaging Kernel corresponding to same AIRS profile on 31 August 2016, color-  
267   coded by pressure level. Averaging kernels with the largest positive sensitivity below  
268   2000 m are from the lowest altitudes.

269

270   **4.2 AIRS Bias correction**

271   TES HDO/H<sub>2</sub>O ratios are biased compared to model and in situ measurements (Worden  
272   et al., 2006, 2007, 2011). We assess whether AIRS HDO has a bias relative to in situ  
273   measurements. As described above, AIRS and TES show a small bias for the HDO/H<sub>2</sub>O  
274   ratio of ~-2.3 per mil (Worden et al., 2019) after a bias correction is applied, so it is  
275   reasonable to see how well in situ and AIRS data agree if the TES bias correction is  
276   applied to the AIRS HDO. Herman et al. (2014) estimated the TES bias  $\delta_{bias}$  by  
277   minimizing the difference between bias-corrected TES and in situ  $\delta D$  with TES operator  
278   applied:

$$\delta_{bias} = 0.00019 \times Pressure - 0.067 \quad (2)$$

279   We apply the TES  $\delta_{bias}$  to the AIRS data to evaluate against ORACLES aircraft data.  
280   There are 446 matched profiles of AIRS and ORACLES within the same  
281   latitude/longitude boxes (Fig. 2), and 110 closely-matched profiles within 0.3 degrees or  
282   approximately 30 km (Fig. 3). Comparisons with averaging kernel applied are shown in  
283   Fig. 5 and Table 2. Over the range of aircraft data, 0 km to 6 km altitude, AIRS  $\delta D$  has a  
284   mean bias of -6.7‰ relative to the aircraft profiles, well within the estimated  
285   measurement uncertainty of both AIRS and the WISPER calibration. This is consistent  
286   with TES  $\delta D$  (Worden et al., 2019; Herman et al., 2014). AIRS lower-tropospheric  $\delta D$   
287   bias is -6.6‰ and RMS 20.9‰ (surface to 800 hPa). In the mid-troposphere, 800 to 500

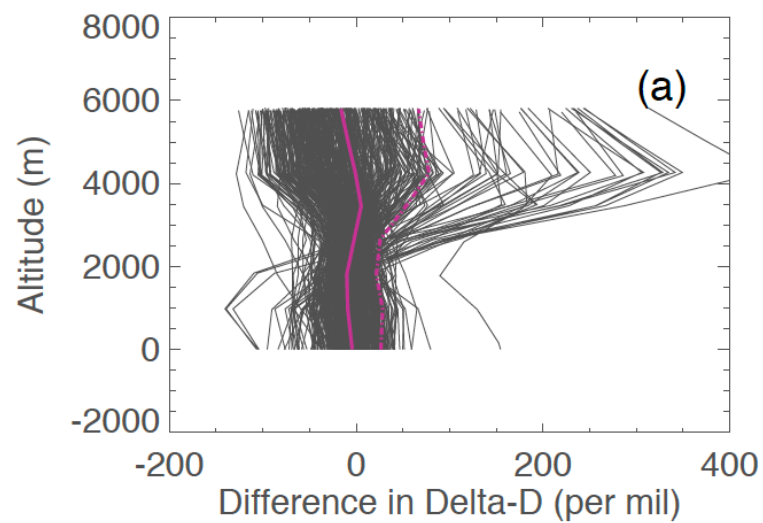


289 hPa, AIRS  $\delta D$  bias is -6.8‰ and RMS 44.9‰.

290

292

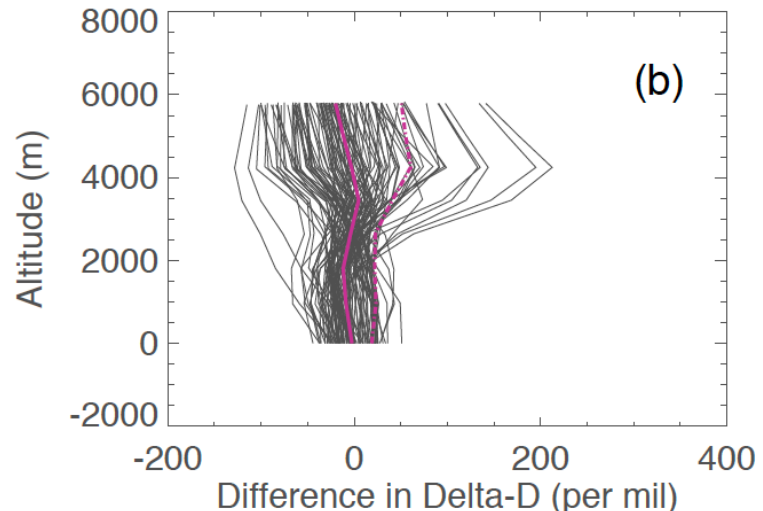
291



293

294 **Figure 5. (a)** AIRS minus ORACLES aircraft  $\delta D$  for the 446 matches within 3 degrees

295 (Fig. 2). Lines are individual profiles (black lines), mean (red solid line) and RMS (red





296 dash dot line).

297 **(b)** AIRS minus ORACLES aircraft  $\delta D$  for the 110 matches within 0.3 degrees (Fig. 3).

298

299 **Table 2.** Summary of satellite-aircraft comparisons for 110 matched pairs in 2016 (Fig. 3). Bias and RMS  
300 (standard deviation) of AIRS  $\delta D$  relative to ORACLE aircraft with averaging kernel applied (“BiasAK”,  
301 “RMSak”), and for AIRS relative to mapped ORACLES aircraft, no averaging kernel (“Bias”, “RMS”).

| Altitude (m) | Pressure (hPa) | BiasAK (‰) | RMSak (‰) | Bias (‰) | RMS (‰) |
|--------------|----------------|------------|-----------|----------|---------|
| 0.01         | 1014.63        | -2.46      | 18.98     | -14.82   | 22.64   |
| 136.61       | 1000.00        | -3.35      | 19.38     | -18.14   | 22.79   |
| 968.87       | 908.51         | -8.86      | 23.39     | -0.31    | 131.50  |
| 1807.71      | 825.40         | -11.80     | 22.05     | 9.77     | 89.68   |
| 2641.34      | 749.89         | -3.89      | 22.63     | -13.24   | 38.07   |
| 3456.36      | 681.29         | 4.89       | 41.03     | -3.66    | 35.98   |
| 4250.29      | 618.97         | -2.96      | 60.63     | 12.52    | 76.03   |
| 5027.62      | 562.34         | -11.87     | 55.15     | -16.62   | 73.75   |
| 5792.12      | 510.90         | -20.09     | 50.61     | -40.41   | 81.22   |

302

303

304 **5. Error estimation**

305 In this section we characterize the error budget for AIRS and assess this error by  
306 comparison with the ORACLES aircraft measurements. Error analysis in optimal  
307 estimation has been described in detail in the literature (Worden et al., 2004, 2006;  
308 Bowman et al., 2004; Rodgers, 2000). The error  $\tilde{x}$  in the estimate of HDO/H<sub>2</sub>O is defined  
309 as the true state  $x$  minus the linear estimate  $\hat{x}$  retrieved by AIRS (e.g., Worden et al.,  
310 2006, Eq. (15)):

$$\tilde{\mathbf{x}} = \mathbf{x} - \hat{\mathbf{x}}. \quad (3)$$

312 Similar to Herman et al. (2014), we define the *estimated error* of the AIRS isotopic ratio

313 HDO/H<sub>2</sub>O, (Eq. 4) as the observation error covariance (Worden et al., 2006):

$$S = G_R S_n G_R^T + G_R \left( \sum_i K_i S_b^i K_i^T \right) G_R^T, \quad (4)$$

315 where  $\mathbf{G}_R = (\mathbf{G}_z^D - \mathbf{G}_z^H)$ ,  $S_n$  is the measurement error covariance, and  $\mathbf{S}_b^i$  is the error

316 covariance due to systematic errors and interference errors. The estimated error is given

317 by the square roots of the diagonal elements of  $\mathbf{S}$ , the best estimate of the AIRS

318 observation error covariance for the HDO/H<sub>2</sub>O retrieval. In the case where AIRS is

319 compared to in situ measurements without the averaging kernel, there is an additional

320 smoothing error.

321

3

322 The estimated error (Eq. 4) is compared to the empirical error calculated from the AIRS-

323 aircraft comparisons. It is seen that the error varies from -20 to +40 per mil (Fig. 6). The

<sup>324</sup> empirical error (AIRS versus aircraft RMS) is similar in magnitude to the estimated error,

but exceeds the estimated error at 500 to 800 hPa in the free troposphere. These

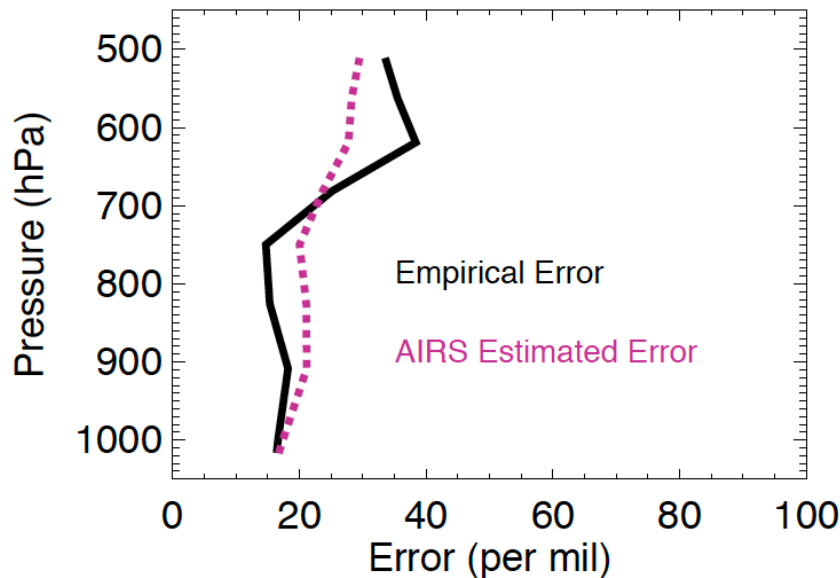
326 differences are likely due to atmospheric variability as we do not have exact matchups

327 between the AIRS data and aircraft measurements.

328



329



330

331 **Figure 6.** AIRS error analysis for coincident AIRS and ORACLES  $\delta D$  on 31 August  
332 2016 shows the empirical error is comparable to the AIRS estimated error. Plotted are the  
333 AIRS  $\delta D$  estimated error also known as AIRS observation error (red dashed line) and the  
334 AIRS  $\delta D$  empirical error (black line).

335

336

## 337 **6. Conclusions**

338 HDO/H<sub>2</sub>O estimates from AIRS single footprint radiances been compared to coincident  
339 in situ airborne measurements on the P-3B Orion aircraft by the Oregon State Water  
340 WISPER system (Water Isotope Spectrometer for Precipitation and Entrainment  
341 Research) over the Southeast Atlantic Ocean. On eight days between 31 Aug and 25 Sep  
342 2016, there are collocated measurements between AIRS and the P-3B aircraft. We have



343 shown that AIRS-only retrievals have sensitivity to HDO from the middle troposphere to  
344 the boundary layer. We demonstrate that AIRS  $\delta D$  has a mean bias of -6.7‰ relative to  
345 aircraft, well within the estimated measurement uncertainty. In the lower troposphere,  
346 1000 to 800 hPa, AIRS  $\delta D$  bias is -6.6‰ and the RMS 20.9‰, consistent with the  
347 calculated uncertainty of 19.1‰. In the mid-troposphere, 800 to 500 hPa, AIRS  $\delta D$  bias  
348 is -6.8‰ and RMS 44.9‰, comparable to the calculated uncertainty of 25.8‰.

349



350   **Code/Data availability.** The ORACLES aircraft data used in the data analysis can be  
351   freely downloaded from the following Digital Object Identifier:  
352   ([http://dx.doi.org/10.5067/Suborbital/ORACLES/P3/2016\\_V1](http://dx.doi.org/10.5067/Suborbital/ORACLES/P3/2016_V1), last access: 22 April  
353   2017). We expect the AIRS-based deuterium data to be publicly released by January  
354   2020. Files in IDL format of the AIRS data shown and forward model output are  
355   available from coauthor John Worden upon request: [john.r.worden@jpl.nasa.gov](mailto:john.r.worden@jpl.nasa.gov).

356

357   **Team list.** Robert L. Herman (RH), John Worden (JW), David Noone (DN), Dean  
358   Henze (DH), Kevin Bowman (KB), Karen Cady-Pereira (KC), Vivienne H. Payne (VP),  
359   Susan S. Kulawik (SK), and Dejian Fu (DF).

360

361   **Author contribution.** RH carried out all steps of aircraft validation, from matching data  
362   and quality filtering to applying observation operator and statistics, while JW provided  
363   satellite-to-satellite validation. JW developed the retrieval strategies for both AIRS and  
364   TES HDO/H<sub>2</sub>O retrievals. DF and SK built the strategies of single AIRS footprint  
365   HDO/H<sub>2</sub>O retrievals into the MUSES algorithm. KC, RH and VP evaluated the  
366   sensitivities of retrievals to the choice of forward model. RH, VP, JW, SK, DF, DN, DH  
367   and KB contributed to the text and interpretation of the results. JW and SK helped in the  
368   estimation of HDO/H<sub>2</sub>O measurement uncertainty, quality flagging and knowledge of the  
369   retrieval process. DN and DH provided ORACLES data, aircraft measurement  
370   uncertainty, and identified profiles in the aircraft data. All authors participated in writing  
371   the manuscript.

372



373    **Competing interests.** The authors declare that they have no conflict of interest.

374

375    **Acknowledgments**

376    Support for R. Herman, J. Worden, S. Kulawik, D. Fu and V. Payne was provided by the  
377    NASA Aura Program. Participation by D. Noone and D. Henze was supported by a grant  
378    from the National Science Foundation Climate and Large-scale Dynamics, and  
379    Atmospheric Chemistry programs (AGS 1564670). Part of the research described in this  
380    paper was carried out by the Jet Propulsion Laboratory, California Institute of  
381    Technology, under a contract with NASA.

382



383    **References**

- 384    Aumann, H. H., Chahine, M. T., Gautier, C., Goldberg, M. D., Kalnay, E., McMillin, L.  
385    M., Revercomb, H., Rosenkranz, P. W., Smith, W. L., Staelin, D. H., Strow, L. L.,  
386    and Susskind, J.: AIRS/AMSU/HSB on the aqua mission: Design, science objectives,  
387    data products, and processing systems. *IEEE Transactions on Geoscience and Remote  
388    Sensing*, 41(2), 253-264, 2003.
- 389    Bailey, A., Blossey, P. N., Noone, D., Nusbaumer, J. & Wood, R. Detecting shifts in  
390    tropical moisture imbalances with satellite-derived isotope ratios in water vapor.  
391    *Journal of Geophysical Research-Atmospheres* 122, 5763–5779 (2017).
- 392    Beer, R.: TES on the Aura Mission: scientific objectives, measurements and analysis  
393    overview, *IEEE T. Geosci. Remote*, 44, 1102-1105, 2006.
- 394    Beer, R., Bowman, K. W., Brown, P. D., Clough, S. A., Eldering, A., Goldman, A.,  
395    Jacob, D. J., Lampel, M., Logan, J. A., Luo, M., Murcray, F. J., Osterman, G. B.,  
396    Rider, D. M., Rinsland, C. P., Rodgers, C. D., Sander, S. P., Shepard, M., Sund, S.,  
397    Ustinov, E. A., Worden, H. M., Worden, J., and Syvertson, M. (Eds.): Tropospheric  
398    Emission Spectrometer (TES) Level 2 Algorithm Theoretical Basis Document, V.  
399    1.16, Jet Propulsion Laboratory, Pasadena, CA, JPL D-16474, 27 June 2002,  
400    available at <http://eospso.gsfc.nasa.gov/atbd-category/53> (last access: 7 December  
401    2010), 2002.
- 402    Beer, R., Glavich, T. A., and Rider, D. M.: Tropospheric emission spectrometer for the  
403    Earth Observing System's Aura satellite, *Appl. Optics*, 40, 2356-2367, 2001.
- 404    Berden, G., Peeters, R., and Meijer, G.: Cavity ring-down spectroscopy: Experimental  
405    schemes and applications, *Int. Rev. Phys. Chem.*, 19, 565-607, doi:



- 406        10.1080/014423500750040627, 2000.
- 407        Berkelhammer, M., Hu, J., Bailey, A., Noone, D., Still, C., Barnard, H., Gochis, D.,
- 408        Hsiao, G., Rahn, T., and Turnipseed, A.: The nocturnal water cycle in an open-
- 409        canopy forest, *J. Geophys. Res.-Atmos.*, 118, 10225-10242, doi:10.1002/jgrd.50701,
- 410        2013.
- 411        Bernath, P. F., McElroy, C. T., Abrams, M. C., Boone, C. D., Butler, M., Camy-Peyret,
- 412        C., Carleer, M., Clerbaux, C., Coheur, P.-F., Colin, R., DeCola, P., DeMazière, M.,
- 413        Drummond, J. R., Dufour, D., Evans, W. F. J., Fast, H., Fussen, D., Gilbert, K.,
- 414        Jennings, D. E., Llewellyn, E. J., Lowe, R. P., Mahieu, E., McConnell, J. C.,
- 415        McHugh, M., McLeod, S. D., Michaud, R., Midwinter, C., Nassar, R., Nichitiu, F.,
- 416        Nowlan, C., Rinsland, C. P., Rochon, Y. J., Rowlands, N., Semeniuk, K., Simon, P.,
- 417        Skelton, R., Sloan, J. J., Soucy, M.-A., Strong, K., Tremblay, P., Turnbull, D.,
- 418        Walker, K. A., Walkty, I., Wardle, D. A., Wehrle, V., Zander, R., and Zou, J.:
- 419        Atmospheric Chemistry Experiment (ACE): Mission overview, *Geophys. Res. Lett.*,
- 420        32, L15S01, doi:10.1029/2005GL022386, 2005.
- 421        Bowman, K. W., Worden, J., Steck, T., Worden, H. M., Clough, S., and Rodgers, C.:
- 422        Capturing time and vertical variability of tropospheric ozone: A study using TES
- 423        nadir retrievals, *J. Geophys. Res.-Atmos.*, 107, 4723, doi:10.1029/2002JD002150,
- 424        2002.
- 425        Bowman, K. W., Rodgers, C. D., Kulawik, S. S., Worden, J., Sarkissian, E., Osterman,
- 426        G., Steck, T., Luo, M., Eldering, A., Shephard, M. W., Worden, H., Lampel, M.,
- 427        Clough, S. A., Brown, P., Rinsland, C., Gunson, M., and Beer, R.: Tropospheric
- 428        Emission Spectrometer: retrieval method and error analysis, *IEEE T. Geosci. Remote*,



- 429        44, 1297-1307, 2006.
- 430        Boxe, C. S., Worden, J. R., Bowman, K. W., Kulawik, S. S., Neu, J. L., Ford, W. C.,  
431        Osterman, G. B., Herman, R. L., Eldering, A., Tarasick, D. W., Thompson, A. M.,  
432        Doughty, D. C., Hoffmann, M. R., and Oltmans, S. J.: Validation of northern latitude  
433        Tropospheric Emission Spectrometer stare ozone profiles with ARC-IONS sondes  
434        during ARCTAS: sensitivity, bias and error analysis, Atmospheric Chemistry and  
435        Physics, doi:10.5194/acp-10-9901-2010, 2010.
- 436        Brown, D., Worden, J., and Noone, D.: Comparison of atmospheric hydrology over  
437        convective continental regions using water vapor isotope measurements from space,  
438        J. Geophys. Res., 113, D15124, doi:10.1029/2007JD009676, 2008.
- 439        Craig, H.: Isotopic Variations in Meteoric Waters, Science, 133, 1702-3, doi:  
440        10.1126/science.133.3465.1702, 1961.
- 441        Dansgaard, W.: Stable isotopes in precipitation, Tellus, 16, 436-68, 1964.
- 442        DeSouza-Machado, S., Strow, L. L., Tangborn, A., Huang, X., Chen, X., Liu, X., Wu, W.  
443        and Yang, Q.: Single-footprint retrievals for AIRS using a fast TwoSlab cloud-  
444        representation model and the SARTA all-sky infrared radiative transfer algorithm,  
445        Atmos. Meas. Tech., 11(1), 529–550, doi:10.1029/2005GL023211, 2018.
- 446        Frankenberg, C., Yoshimura, K., Warneke, T., Aben, I., Butz, A., Deutscher, N., Griffith,  
447        D., Hase, F., Notholt, J., Schneider, M., Schrijver, H., and Röckmann, T.: Dynamic  
448        Processes Governing Lower-Tropospheric HDO/H<sub>2</sub>O Ratios as Observed from Space  
449        and Ground, Science, 325, 1374, DOI: 10.1126/science.1173791, 2009.
- 450        Fu, D., Kulawik, S. S., Miyazaki, K., Bowman, K. W., Worden, J. R., Eldering, A.,  
451        Livesey, N. J., Teixeira, J., Irion, F. W., Herman, R. L., Osterman, G. B., Liu, X.,



- 452 Levelt, P. F., Thompson, A. M., and Luo, M.: Retrievals of tropospheric ozone  
453 profiles from the synergism of AIRS and OMI: methodology and validation, *Atmos.*  
454 *Meas. Tech.*, 11, 5587-5605, <https://doi.org/10.5194/amt-11-5587-2018>, 2018.
- 455 Fu, D., Bowman, K. W., Worden, H. M., Natraj, V., Worden, J. R., Yu, S., Veefkind, P.,  
456 Aben, I., Landgraf, J., Strow, L., and Han, Y.: High-resolution tropospheric carbon  
457 monoxide profiles retrieved from CrIS and TROPOMI, *Atmos. Meas. Tech.*, 9, 2567-  
458 2579, <https://doi.org/10.5194/amt-9-2567-2016>, 2016.
- 459 Fu, D., Worden, J. R., Liu, X., Kulawik, S. S., Bowman, K. W., and Natraj, V.:  
460 Characterization of ozone profiles derived from Aura TES and OMI radiances,  
461 *Atmos. Chem. Phys.*, 13, 3445-3462, <https://doi.org/10.5194/acp-13-3445-2013>,  
462 2013.
- 463 Fu, R.: *et al.* Increased dry-season length over southern Amazonia in recent decades and  
464 its implication for future climate projection. *Proceedings of the National Academy of*  
465 *Sciences of the United States of America* **110**, 18110–18115 (2013).
- 466 Galewsky, J., Steen-Larsen, H.-C., Field, R. D., Worden, J., Risi, C., and Schneider, M.:  
467 [Stable isotopes in atmospheric water vapor and applications to the hydrologic cycle,](#)  
468 *Rev. Geophys.*, 54, 4, 809-65, 2016.
- 469 Good, S. P., Noone, D., Bowen, G., Hydrologic connectivity constrains partitioning of  
470 global terrestrial water fluxes, *Science*, 349, 6244, 175-177, 2015.
- 471 Gupta, P., Noone, D., Galewsky, J., Sweeny, C., and Vaughn, B. H.: Demonstration of  
472 high precision continuous measurements of water vapor isotopologues in laboratory  
473 and remote field deployments using WS-CRDS technology, *Rapid Commun. Mass*  
474 *Sp.*, 23, 2534-2542, doi: 10.1002/rcm.4100, 2009.



- 475 Henze, D., Toohey, D., and Noone, D.: The Water Isotope Spectrometer for Precipitation  
476 and Entrainment Research (WISPER), in prep., 2019.
- 477 Herbin, H., Hurtmans, D., Turquety, S., Wespes, C., Barret, B., Hadji-Lazaro, J., Clerbaux,  
478 C., and Coheur, P.-F.: Global distributions of water vapour isotopologues retrieved  
479 from IMG/ADEOS data, *Atmos. Chem. Phys.*, 7, 3957–3968, doi:10.5194/acp-7-3957-  
480 2007, 2007.
- 481 Herbin, H., Hurtmans, D., Clerbaux, C., Clarisse, L., and Coheur, P.-F.:  $\text{H}_2^{16}\text{O}$  and HDO  
482 measurements with IASI/MetOp, *Atmos. Chem. Phys.*, 9, 9433-9447,  
483 doi:10.5194/acp-9-9433-2009, 2009.
- 484 Herman, R. L., Cherry, J. E., Young, J., Welker, J. M., Noone, D., Kulawik, S. S., and  
485 Worden, J.: Aircraft validation of Aura Tropospheric Emission Spectrometer retrievals  
486 of HDO/ $\text{H}_2\text{O}$ , *Atmos. Meas. Tech.*, 7, 3127–3138, 2014, 2014.
- 487 Herman, R. L., and Kulawik, S. S. (Eds.): Tropospheric Emission Spectrometer TES Level  
488 2 (L2) Data User's Guide, D-38042, version 7.0, Jet Propulsion Laboratory, California  
489 Institute of Technology, Pasadena, CA, available at:  
490 [https://eosweb.larc.nasa.gov/project/tes/guide/TESDataUsersGuideV7\\_0\\_Sep\\_27\\_2018\\_FV-2.pdf](https://eosweb.larc.nasa.gov/project/tes/guide/TESDataUsersGuideV7_0_Sep_27_2018_FV-2.pdf) (last access: 18 October 2018), 2018.
- 492 Herman, R. L., and Osterman, G. B. (Eds.): Tropospheric Emission Spectrometer Data  
493 Validation Report (Version F08\_11 data), D-33192, Version 7.0, Jet Propulsion  
494 Laboratory, California Institute of Technology, Pasadena, CA, available at:  
495 [https://eosweb.larc.nasa.gov/sites/default/files/project/tes/readme/TES\\_Validation\\_Report\\_v7\\_Final.pdf](https://eosweb.larc.nasa.gov/sites/default/files/project/tes/readme/TES_Validation_Report_v7_Final.pdf) (last access: 15 October 2018), 2018.
- 497 Irion, F. W., Kahn, B. H., Schreier, M. M., Fetzer, E. J., Fishbein, E., Fu, D., Kalmus, P.,



- 498 Wilson, R. C., Wong, S. and Yue, Q.: Single-footprint retrievals of temperature,  
499 water vapor and cloud properties from AIRS, *Atmos. Meas. Tech.*, 11(2), 971–995,  
500 doi:10.1111/12.615244, 2018.
- 501 Irion, F. W., Moyer, E. J., Gunson, M. R., Rinsland, C. P., Yung, Y. L., Michelsen, H. A.,  
502 Salawitch, R. J., Chang, A. Y., Newchurch, M. J., Abbas, M. M., Abrams, M. C., and  
503 Zander, R.: Stratospheric observations of CH<sub>3</sub>D and HDO from ATMOS infrared  
504 solar spectra: Enrichments of deuterium in methane and implications for HD,  
505 *Geophys. Res. Lett.*, 23(17), 2381-4, 1996.
- 506 Kuang, Z., Toon, G. C., Wennberg, P. O., and Yung, Y. L.: Measured HDO/H<sub>2</sub>O ratios  
507 across the tropical tropopause, *Geophys. Res. Lett.*, 30(7), 1372,  
508 doi:10.1029/2003GL017023, 2003.
- 509 Kulawik, S. S., Bowman, K. W., Luo, M., Rodgers, C. D., and Jourdain, L.: Impact of  
510 nonlinearity on changing the a priori of trace gas profile estimates from the  
511 Tropospheric Emission Spectrometer (TES), *Atmos. Chem. Phys.*, 8, 3081-92,  
512 doi:10.5194/acp-8-3081-2008, 2008.
- 513 Kulawik, S. S., Worden, H., Osterman, G., Luo, M., Beer, R., Worden, J., Bowman, K.,  
514 Eldering, A., Lampel, M., Steck, T., and Rodgers, C.: TES Atmospheric Profile  
515 Retrieval Characterization: An orbit of simulated observations, *IEEE T. Geosci.  
516 Remote*, 44, 1324-1333, 2006.
- 517 Lacour, J.-L., Risi, C., Clarisse, L., Bony, S., Hurtmans, D., Clerbaux, C., and Coheur,  
518 P.-F.: Mid-tropospheric δD observations from IASI/MetOp at high spatial and  
519 temporal resolution, *Atmos. Chem. Phys.*, 12, 10817–10832, doi:10.5194/acp-12-  
520 10817-2012, 2012.



- 521 Lee, J., Worden, J., Noone, D., Bowman, K., Eldering, A., LeGrande, A., Li, J. L. F.,  
522 Schmidt, G., and Sodemann, H.: Relating tropical ocean clouds to moist processes  
523 using water vapor isotope measurements, *Atmos. Chem. Phys.*, 11, 741-752,  
524 doi:10.5194/acp-11-741-2011, 2011.
- 525 Lossow, S., Steinwagner, J., Urban, J., Dupuy, E., Boone, C. D., Kellmann, S., Linden,  
526 A., Kiefer, M., Grabowski, U., Glatthor, N., Hopfner, M., Rockmann, T., Murtagh, D.  
527 P., Walker, K. A., Bernath, P. F., von Clarmann, T., and Stiller, G. P.: Comparison of  
528 HDO measurements from Envisat/MIPAS with observations by Odin/SMR and  
529 SCISAT/ACE-FTS, *Atmos. Meas. Tech.*, 4, 1855-1874, doi:10.5194/amt-4-1855-  
530 2011, 2011.
- 531 Moncet, J.-L., Uymin, G., Liang, P., and Lipton, A. E.: Fast and accurate radiative  
532 transfer in the thermal regime by simultaneous optimal spectral sampling over all  
533 channels, *J. Atmos. Sci.*, 72, 2622–2641, <https://doi.org/10.1175/JAS-D-14-0190.1>,  
534 2015.
- 535 Moncet, J.-L., Uymin, G., Lipton, A. E., and Snell, H. E.: Infrared radiance modeling by  
536 optimal spectral sampling, *J. Atmos. Sci.*, 65, 3917–3934,  
537 <https://doi.org/10.1175/2008JAS2711.1>, 2008.
- 538 Moyer, E. J., Irion, F. W., Yung, Y. L., and Gunson, M. R.: ATMOS stratospheric  
539 deuterated water and implications for troposphere-stratosphere transport, *Geophys.  
540 Res. Lett.*, 23(17), 2385-8, 1996.
- 541 Murtagh, D., Frisk, U., Merino, F., Ridal, M., Jonsson, A., Stegman, J., Witt, G.,  
542 Eriksson, P., Jiménez, C., Megie, G., de la Noë, J., Ricaud, P., Baron, P., Pardo, J. R.,  
543 Hauchcorne, A., Llewellyn, E. J., Degenstein, D. A., Gattinger, R. L., Lloyd, N. D.,



- 544      Evans, W. F. J., McDade, I. C., Haley, C. S., Sioris, C., von Savigny, C., Solheim, B.  
545      H., McConnell, J. C., Strong, K., Richardson, E. H., Leppelmeier, G. W., Kyrölä, E.,  
546      Auvinen, H., and Oikarinen, L.: An overview of the Odin atmospheric mission, Can.  
547      J. Phys., 80, 309-319, doi:10.1139/p01-157, 2002.  
548      Noone, D.: Pairing Measurements of the Water Vapor Isotope Ratio with Humidity to  
549      Deduce Atmospheric Moistening and Dehydration in the Tropical Midtroposphere,  
550      Journal of Climate, 25(13), 4476-4494, 2012.  
551      Noone, D., Galewsky, J., Sharp, Z. D., Worden, J., Barnes, J., Baer, D., Bailey, A.,  
552      Brown, D. P., Christensen, L., Crosson, E., Dong, F., Hurley, J. V., Johnson, L. R.,  
553      Strong, M., Toohey, D., Van Pelt, A., and Wright, J. S.: Properties of air mass mixing  
554      and humidity in the subtropics from measurements of the D/H isotope ratio of water  
555      vapor at the Mauna Loa Observatory, J. Geophys. Res.-Atmos., 116, D22113,  
556      doi:10.1029/2011JD015773, 2011.  
557      O'Keefe, A., and Deacon, D. A. G.: Cavity ringdown optical spectrometer for absorption  
558      measurements using pulsed laser sources, Rev. Sci. Instrum., 59, 2544; doi:  
559      10.1063/1.1139895, 1988.  
560      ORACLES Science Team: Suite of Aerosol, Cloud, and Related Data Acquired Aboard  
561      P3 During ORACLES 2016, Version 1, NASA Ames Earth Science Project Office,  
562      [http://dx.doi.org/10.5067/Suborbital/ORACLES/P3/2016\\_V1](http://dx.doi.org/10.5067/Suborbital/ORACLES/P3/2016_V1), 2017.  
563      Pagano, T. S., Aumann, H. H., Hagan, D. E., and Overoye, K.: Prelaunch and in-flight  
564      radiometric calibration of the Atmospheric Infrared Sounder (AIRS), IEEE  
565      Transactions on Geoscience and Remote Sensing, 41(2), 265-273, 2003.  
566      Pagano, T. S., Aumann, H., Schindler, R., Elliott, D., Broberg, S., Overoye, K., Weiler,



- 567 M.: Absolute Radiometric Calibration Accuracy of the Atmospheric Infrared  
568 Sounder, Proc SPIE, 7081-46, San Diego, California, August, 2008.  
569 Pougatchev, N., August, T., Calbet, X., Hultberg, T., Oduleye, O., Schlüssel, P., Stiller,  
570 B., St. Germain, K., and Bingham, G.: IASI temperature and water vapor retrievals –  
571 error assessment and validation, Atmos. Chem. Phys., 9, 6453-6458, doi:10.5194/acp-  
572 9-6453-2009, 2009.  
573 Randel, W. J., Moyer, E., Park, M., Jensen, E., Bernath, P., Walker, K., and Boone, C.:  
574 Global variations of HDO and HDO/H<sub>2</sub>O ratios in the upper troposphere and lower  
575 stratosphere derived from ACE-FTS satellite measurements, J. Geophys. Res.-  
576 Atmos., 117, D06303, doi:10.1029/2011JD016632, 2012.  
577 Rienecker, M. M., Suarez, M. J., Todling, R., Bacmeister, J., Takacs, L., Liu, H.-C., Gu,  
578 W., Sienkiewicz, M., Koster, R. D., Gelaro, R., and Stajner, I., and Nielson, J. E.: The  
579 GEOS-5 Data Assimilation System: Documentation of Versions 5.0, 5.1.0 and 5.2.0,  
580 NASA TM 104606, 27, NASA Technical Report Series on Global Modeling and Data  
581 Assimilation, 2008.  
582 Rinsland, C. P., Gunson, M. R., Foster, J. C., Toth, R. A., Farmer, C. B., and Zander, R.:  
583 Stratospheric Profiles of Heavy Water Vapor Isotopes and CH<sub>3</sub>D From Analysis of  
584 the ATMOS Spacelab 3 Infrared Solar Spectra, J. Geophys. Res., 96, 1057-1068,  
585 1991.  
586 Rodgers, C. D.: Inverse Methods for Atmospheric Sounding: Theory and Practice, World  
587 Science, London, 2000.  
588 Rodgers, C. D., and Connor, B. J.: Intercomparison of Remote Sounding Instruments, J.  
589 Geophys. Res., 108, 4116, doi: 10.1029/2002JD002299, 2003.



- 590 Schneider, M., and Hase, F.: Optimal estimation of tropospheric H<sub>2</sub>O and δD with  
591 IASI/METOP, *Atmos. Chem. Phys.*, 11, 11207-220, doi: 10.5194/acp-11-11207-  
592 2011, 2011.
- 593 Schneider, M., Hase, F., and Blumenstock, T.: Ground-based remote sensing of  
594 HDO/H<sub>2</sub>O ratio profiles: Introduction and validation of an innovative retrieval  
595 approach, *Atmos. Chem. Phys.*, 6, 4705–4722, doi:10.5194/acp-6-4705-2006, 2006.
- 596 Schneider, M., Toon, G., Blavier, J.-F., Hase, F., and Leblanc, T.: H<sub>2</sub>O and δD profiles  
597 remotely-sensed from ground in different spectral infrared regions, *Atmos. Meas.  
Tech.*, 3, 1599–1613, doi:10.5194/amt-3-1599-2010, 2010.
- 599 Schoeberl, M. R., Douglass, A. R., Hilsenrath, E., Bhartia, P. K., Barnett, J., Beer, R.,  
600 Waters, J., Gunson, M., Froidevaux, L., Gille, J., Levelt, P. F., and DeCola, P.:  
601 Overview of the EOS Aura Mission, *IEEE T. Geosci. Remote*, 44, 1066-1077, 2006.
- 602 Shephard, M. W., Herman, R. L., Fisher, B. M., Cady-Pereira, K. E., Clough, S. A.,  
603 Payne, V. H., Whiteman, D. N., Comer, J. P., Vömel, H., Miloshevich, L. M., Forno,  
604 R., Adam, M., Osterman G. B., Eldering, A., Worden, J. R., Brown, L. R., Worden,  
605 H. M., Kulawik, S. S., Rider, D. M., Goldman, A., Beer, R., Bowman, K. W.,  
606 Rodgers, C. D., Luo, M., Rinsland, C. P., Lampel, M., and Gunson, M. R.:  
607 Comparison of Tropospheric Emission Spectrometer (TES) water vapor retrievals  
608 with in situ measurements, *J. Geophys. Res.*, 113, D15824,  
609 doi:10.1029/2007JD008822, 2008.
- 610 Steinwagner, J., Fueglistaler, S., Stiller, G., von Clarmann, T., Kiefer, M., Borsboom, P.  
611 P., van Delden, A., and Rockmann, T.: Tropical dehydration processes constrained by  
612 the seasonality of stratospheric deuterated water, *Nat. Geosci.*, 3, 262-266, 2010.



- 613 Steinwagner, J., Milz, M., von Clarmann, T., Glatthor, N., Grabowski, U., Hopfner, M.,  
614 Stiller, G. P., and Rockmann, T.: HDO measurements with MIPAS, *Atmos. Chem.  
615 Phys.*, 7, 2601-2615, doi:10.5194/acp-7-2601-2007, 2007.
- 616 Tobin, C. D., Revercomb, H. E., Knuteson, R. O., Lesht, B. M., Strow, L. L., Hannon, S.  
617 E., Feltz, W. F., Moy, L. A., Fetzer, E. J., and Cress, T. S.: Atmospheric Radiation  
618 Measurement site atmospheric state best estimates for Atmospheric Infrared Sounder  
619 temperature and water vapor retrieval validations, *J. Geophys. Res.*, 111, D09S14,  
620 doi:10.1029/2005JD006103, 2006.
- 621 Urban, J., Lautie, N., Murtagh, D., Eriksson, P., Kasai, Y., Lossow, S., Dupuy, E., de la  
622 Noe, J., Frisk, U., Olberg, M., Le Flochmoen, E., and Ricaud, P.: Global observations  
623 of middle atmospheric water vapour by the Odin satellite: An overview, *Planet. Space  
624 Sci.*, 55, 1093-1102, doi:10.1016/j.pss.2006.11.021, 2007.
- 625 Worden, H. M., Logan, J. A., Worden, J. R., Beer, R., Bowman, K., Clough, S. A.,  
626 Eldering, A., Fisher, B. M., Gunson, M. R., Herman, R. L., Kulawik, S. S., Lampel,  
627 M. C., Luo, M., Megretskaya, I. A., Osterman, G. B., and Shephard, M. W.:  
628 Comparisons of Tropospheric Emission Spectrometer (TES) ozone profiles to  
629 ozonesondes: Methods and initial results, *J. Geophys. Res.*, 112, D03309,  
630 doi:10.1029/2006JD007258, 2007.
- 631 Worden, J., Bowman, K., Noone, D., Beer, R., Clough, S., Eldering, A., Fisher, B.,  
632 Goldman, A., Gunson, M., Herman, R., Kulawik, S. S., Lampel, M., Luo, M.,  
633 Osterman, G., Rinsland, C., Rodgers, C., Sander, S., Shephard, M., and Worden, H.:  
634 Tropospheric Emission Spectrometer observations of the tropospheric HDO/H<sub>2</sub>O  
635 ratio: Estimation approach and characterization, *J. Geophys. Res.*, 111, D16309,



- 636        doi:10.1029/2005JD006606, 2006.
- 637        Worden, J., Kulawik, S., Frankenberg, C., Payne, V., Bowman, K., Cady-Pereira, K.,  
638        Wecht, K., Lee, J.-E., and Noone, D.: Profiles of CH<sub>4</sub>, HDO, H<sub>2</sub>O, and N<sub>2</sub>O with  
639        improved lower tropospheric vertical resolution from Aura TES radiances, Atmos.  
640        Meas. Tech., 5, 397–411, doi:10.5194/amt-5-397-2012, 2012.
- 641        Worden, J. R., Kulawik, S. S., Fu, D., Payne, V. H., Lipton, A. E., Polonsky, I., He, Y.,  
642        Cady-Pereira, K., Moncet, J.-L., Herman, R. L., Irion, F. W., and Bowman, K. W.:  
643        Characterization and evaluation of AIRS-based estimates of the deuterium content of  
644        water vapor, Atmos. Meas. Tech., 12, 2331-2339, <https://doi.org/10.5194/amt-12-2331-2019>, 2019.
- 645        Worden, J., Kulawik, S., Shephard, M., Clough, S., Worden, H., Bowman, K., and  
646        Goldman, A.: Predicted errors of Tropospheric Emission Spectrometer nadir  
647        retrievals from spectral window selection, J. Geophys. Res., 109, D09308,  
648        doi:10.1029/2004JD004522, 2004.
- 649        Worden, J., Noone, D., Bowman, K., and TES science team and data contributors:  
650        Importance of rain evaporation and continental convection in the tropical water cycle,  
651        Nature, 445, 528-532, doi:10.1038/nature05508, 2007.
- 652        Worden, J., Noone, D., Galewsky, J., Bailey, A., Bowman, K., Brown, D., Hurley, J.,  
653        Kulawik, S., Lee, J., and Strong, M.: Estimate of bias in Aura TES HDO/H<sub>2</sub>O profiles  
654        from comparison of TES and in situ HDO/H<sub>2</sub>O measurements at the Mauna Loa  
655        observatory, Atmos. Chem. Phys., 11, 4491-503, doi: 10.5194/acp-11-4491-2011,  
656        2011.
- 657        Worden, J., Wecht, K., Frankenberg, C., Alvarado, M., Bowman, K., Kort, E., Kulawik,



- 659 S., Lee, M., Payne, V., and Worden, H.: CH<sub>4</sub> and CO distributions over tropical fires  
660 during October 2006 as observed by the Aura TES satellite instrument and modeled  
661 by GEOS-Chem, Atmos. Chem. Phys., 13, 3679–3692,<https://doi.org/10.5194/acp-13-3679-2013>, 2013.
- 663 Wright, J. S., Fu, R., Worden, J. R., Chakraborty, S., Clinton, N. E., Risi, C., Sun, U., and  
664 Yin, L., Rainforest-initiated wet season onset over the southern Amazon, Proc. Nat.  
665 Acad. Sciences, 114, 32, 8481-6, 2017.
- 666 Zakharov, V. I., Imasu, R., Gribanov, K. G., Hoffmann, G., and Jouzel, J.: Latitudinal  
667 distribution of the deuterium to hydrogen ratio in the atmospheric water vapor  
668 retrieved from IMG/ADEOS data, Geophys. Res. Lett., 31, L12104,  
669 doi:10.1029/2004GL019433, 2004.
- 670 Zhu, Y., and Gelaro, R.: Observation sensitivity calculations using the adjoint of the  
671 Gridpoint Statistical Interpolation (GSI) analysis system, Mon. Weather Rev., 136,  
672 335-351. doi: 10.1175/MWR3525.1, 2008.